15673

Composite Bridges: Health Monitoring with the Diagnostic Prognostic System (DPS) and an Evaluation of a Temporary Field Repair System

Frank Abdi†*, Rashid Miraj†, Ayman Mosallam‡, and Jian-Juei Wang§, and Ramki Iyer ¥

† Alpha Star Corporation, Long Beach, California USA
‡ University of California at Irvine, California, USA
§ The Boeing Company, Huntington Beach, California, USA
¥ US Army TARDEC, Detroit, Michigan, USA

Abstract

Composite bridges offer many advantages compared to current steel and aluminum bridges including their lightweight and superior corrosion resistance properties. This paper presents the results of a comprehensive on-going research program to develop innovative field repair techniques for composite bridges. In previous papers, information regarding calibration of material properties and fatigue testing with composite treadways was presented. Areas explored to date have been health monitoring with the Diagnostic Prognostic System (DPS) and a structural evaluation of a temporary field repair system. Health monitoring of a composite beam with DPS entailed comparing live strain data to archived strained data in three different locations. For temporary field repairs, a family of composite chords was subjected simple ramp loads in search of ultimate strength. As such, composite bridge specimens showcased their strengths, heralded the viability of virtual testing, highlighted the efficacy of field repair, and confirmed the merits of health monitoring. Keywords: Progressive failure analysis, GENOA, Composite bridge, DPS, Repair

1. Introduction

In recent years, the use of advanced composites to build bridges and bridge components for both military and civilian applications has become an attractive topic of research for many structural engineers (Mosallam 2003, Abdi 2003). Composite bridges provide numerous attractive features. The lightweight characteristic of composites is desirable and essential to achieve the goal of rapid operational mobility. However a fatigue-cycled bridge may have damages that are due to punctures, impact loads and deployment issues related to handling, dropping or dragging. (Abdi 2003).

Internal damage in composites is often initiated as matrix cracking due to tensile stresses transverse to fiber orientation. Nevertheless, damage initiation and progression characteristics for composite structures are diverse. In the presence of stress concentrations, or defects, initial damage may also include fiber fracture. Further degradation takes the form of additional fiber fractures that usually lead to structural failure. Due to the many possibilities with material combinations, composite geometry, fiber orientations, and loading conditions, it is essential to have an effective computational capability to predict the behavior of composite structures for any loading, geometry, composite material combinations, and boundary conditions. The predictions of damage initiation, growth, accumulation, and propagation to fracture are important

Report Documentation Page

Form Approved
OMB No. 0704-0188

1. REPORT DATE	2. REPORT TYPE	3. DATES COVERED
28 MAR 2006	**Journal Article**	**28-03-2006 to 28-03-2006**

4. TITLE AND SUBTITLE
COMPOSITE BRIDGES: HEALTH MONITORING WITH THE DIAGNOSTIC PROGNOSTIC SYSTEM (DPS) AND AN EVALUATION OF A TEMPORARY FIELD REPAIR SYSTEM

5a. CONTRACT NUMBER
5b. GRANT NUMBER
5c. PROGRAM ELEMENT NUMBER

6. AUTHOR(S)
Ramki Iyer; jian-Juei Wang; Ayman Mosallam; Rashid Miraj; Frank Abdi

5d. PROJECT NUMBER
5e. TASK NUMBER
5f. WORK UNIT NUMBER

7. PERFORMING ORGANIZATION NAME(S) AND ADDRESS(ES)
U.S. Army TARDEC ,6501 E.11 Mile Rd,Warren,MI,48397-5000

8. PERFORMING ORGANIZATION REPORT NUMBER
#15673

9. SPONSORING/MONITORING AGENCY NAME(S) AND ADDRESS(ES)
U.S. Army TARDEC, 6501 E.11 Mile Rd, Warren, MI, 48397-5000

10. SPONSOR/MONITOR'S ACRONYM(S)
TARDEC

11. SPONSOR/MONITOR'S REPORT NUMBER(S)
#15673

12. DISTRIBUTION/AVAILABILITY STATEMENT
Approved for public release; distribution unlimited

13. SUPPLEMENTARY NOTES
JEC CONFERENCE , PARIS

14. ABSTRACT
Composite bridges offer many advantages compared to current steel and aluminum bridges including their lightweight and superior corrosion resistance properties. This paper presents the results of a comprehensive on-going research program to develop innovative field repair techniques for composite bridges. In previous papers, information regarding calibration of material properties and fatigue testing with composite treadways was presented. Areas explored to date have been health monitoring with the Diagnostic Prognostic System (DPS) and a structural evaluation of a temporary field repair system. Health monitoring of a composite beam with DPS entailed comparing live strain data to archived strained data in three different locations. For temporary field repairs, a family of composite chords was SUbjected simple ramp loads in search of ultimate strength. As such, composite bridge specimens showcased their strengths, heralded the viability of virtual testing, highlighted the efficacy of field repair, and confirmed the merits of health monitoring. Keywords: Progressive failure analysis, GENOA Composite bridge, DPS, Repair

15. SUBJECT TERMS

16. SECURITY CLASSIFICATION OF:			17. LIMITATION OF ABSTRACT	18. NUMBER OF PAGES	19a. NAME OF RESPONSIBLE PERSON
a. REPORT	b. ABSTRACT	c. THIS PAGE			
unclassified	**unclassified**	**unclassified**	**Same as Report (SAR)**	**15**	

to evaluate the load carrying capacity and reliability of composite structures. Quantification of the structural fracture resistance is also required to evaluate the durability/life of composite structures. A computational simulation method has been developed for this purpose. The method is able to simulate damage initiation, damage growth, and fracture in composites under various loading, considering also the effects of residual stresses and environmental conditions (Chamis 1996). The objective of the paper is to integrate this simulation capability into health monitoring. The first part of this study is involved with the DPS. In this instance, DPS is used to monitor the health of a composite beam. Virtual testing is called upon to provide an estimate of the behavior and is supplemented by actual experimental values of strain taken from the composite beam. In the second part of this study, undamaged, damaged and repaired composite chords are subjected to simple ramp loads in search of ultimate strength. The resulting values of strength serve to gauge the efficacy of the repair methodology.

2. Methodology

2.1 *Progressive Fatigue Failure Analysis*

The simulation analysis for durability, reliability, and risk assessment is based on an enhanced software system technology, the General Optimiser Analyzer (GENOA), which takes a full-scale finite element model and breaks the material properties down to the microscopic level, where material properties are updated for each iteration, reflecting any changes resulting from damage or crack propagation. The hierarchical approach implemented in GENOA allows integration of a wide range of specialized programs, from micro to macro, into an existing verified progressive failure and probabilistic analysis tool. This makes it possible to accurately evaluate the behavior Polymer Matrix Composites (PMC) structures by way of progressive failure analysis and virtual testing, which is based on the physics and micro/macro mechanics of materials, manufacturing processes, available data, and service environments. This approach takes progressive damage and fracture processes into account and accurately assesses reliability by predicting failure initiation and progression based on constituent material properties. The life prediction codes utilize and integrate: 1) finite element structural analysis, 2) micro-mechanics, and fracture mechanics options, 3) damage progression tracking, 4) probabilistic risk assessment, 5) minimum damage design optimization, and 6) material characterization codes to scale up the effects of local damage mechanisms to the structure level to evaluate overall performance and integrity. A significant advantage of using a life prediction tool in the design process is that the number of experimental tests at the component and substructure levels can be substantially reduced. The damage progression module relies on a composite mechanics code (Murthy 1986) for composite micromechanics, macro-mechanics, laminate analysis, as well as cyclic loading durability analysis, and calls a finite element analysis module that uses anisotropic thick shell elements to model laminated composites (Nakazawa 1987).

Imposing failure criteria locally within each micromechanics sub-volume carries out progressive damage and fracture simulations. Micromechanics sub-volumes are obtained by subdividing each micromechanics volume into regions with characteristic fiber configuration. Within each sub-volume, local coordinate orientation in the material coordinate systems are identified. At each individual load step, the stresses and strains obtained through 3D woven composite micro stress analysis are checked according to distinct failure criteria. The first twelve failure modes are associated with the positive and negative limits of the six local stress components in the

material direction as follows:

$S_{l11C} < \sigma_{l11} < S_{l11T}$, where S_{l11C} is longitudinal compressive strength and S_{l11T} is longitudinal tensile strength 1(a)

$S_{l33C} < \sigma_{l33} < S_{l33T}$, where S_{l22C} is transverse compressive strength and S_{l22T} is transverse tensile strength 1(b)

$S_{l33C} < \sigma_{l33} < S_{l33T}$, where S_{l33C} is normal compressive strength and S_{l33T} is normal tensile strength 1(c)

$S_{l12(-)} < \sigma_{l12} < S_{l12(+)}$, where $S_{l12(-)}$ is in-plane negative shear strength and $S_{l12(+)}$ is in-plane positive shear strength 1(d)

$S_{l23(-)} < \sigma_{l23} < S_{l23(+)}$, where $S_{l23(-)}$ is transverse-normal negative shear strength and $S_{l23(+)}$ is transverse-normal positive shear strength 1(e)

$S_{l13(-)} < \sigma_{l13} < S_{l13(+)}$, where $S_{l13(-)}$ is longitudinal-normal negative shear strength and $S_{l13(+)}$ is longitudinal-normal shear strength 1(f)

The thirteenth failure mode is a combined stress failure criterion, or a modified distortion energy (MDE) failure criterion that is obtained by modifying the usual distortion energy failure criterion. The modification takes into account the significant differences in the stress limits of the longitudinal and transverse directions of an orthotropic composite ply. Each component of ply stress is normalized with respect to its limiting strength. The MDE failure criterion has been demonstrated to be a good predictor of combined stress failure in composites. It may be considered as a variation of the Tsai-Hill theory (Tsai 1968, Hill 1950). The MDE failure criterion (Chamis 1969) can be expressed as:

$$\left(\frac{\sigma_{l11\alpha}}{S_{l11\alpha}}\right)^2 + \left(\frac{\sigma_{l22\beta}}{S_{l22\beta}}\right)^2 - K_{l12\alpha\beta}\frac{\sigma_{l11\alpha}}{S_{l11\alpha}}\frac{\sigma_{l22\beta}}{S_{l22\beta}} + \left(\frac{\sigma_{l12S}}{S_{l12S}}\right)^2 < 1 \qquad (2)$$

where α and β indicate tensile or compressive stresses, $S_{l11\alpha}$ is the local longitudinal strength in tension or compression, $S_{l22\beta}$ is the transverse strength in tension or compression, and the directional interaction factor is defined as:

$$K_{l12\alpha\beta} = K'_{l12\alpha\beta}\frac{(1+4\upsilon_{12}-\upsilon_{13})E_{12}+(1-\upsilon_{23})E_{11}}{[E_{11}E_{22}(2+\upsilon_{12}+\upsilon_{13})(2+\upsilon_{21}+\upsilon_{23})]^{1/2}} \qquad (3)$$

where $K'_{l12\alpha\beta}$ is a theory-experiment correlation factor. The directional interaction factor reduces to unity for homogeneous isotropic materials.

2.2 *DPS Background*

The health monitoring of civil engineering infrastructure has grown rapidly over the last decade. While most systems have sought to provide information as to the state or health of a structure, few have attempted to prognosticate events and estimate residual capacity. The DPS was developed to address this shortfall. DPS was created as part of program that sought innovative approaches and new techniques to repair composite bridges in the field. Specifically, DPS provides a mechanism to capture strain data from a remotely located structure in response to a live loading event. Next, DPS remotely transmits the data from the structure to a web server hosting the Collaborative Virtual Testing (CVT) software. The central data server not only supports GENOA analysis but also maintains a vast arsenal of archived simulations, including multiple progressive failure models of the composite bridge in question and specific information

on maximum threshold strains unique to the that structure. Thirdly, a CVT operator, but generally anyone with access to CVT, may compare live strain data transmitted from the field to simulated maximum threshold strains and, as such, identify areas of damage or failure. Here, it should be noted that CVT supports many GENOA features, which allow a pro-active operator to extract vast amounts of information and draw numerous conclusions from simulation models, related to the remote structure, that have experienced damage. In all there are nine steps associated with DPS, as identified in Figure 1, with the final features providing insight into residual strength as a result of repair. DPS combines real-time remote sensing with the power of virtual testing and progressive failure analysis. DPS not only identifies damage but also determines residual properties and finds the best possible repair solution from a mix of available materials.

DPS is dependent upon four core technologies. These technologies include virtual testing and progressive failure analysis with GENOA; event driven data interrogation of serially multiplexed, optical Fiber-Bragg strain sensors; Internet supported data transmission via satellite or cellular networks; and data processing and data storage through Collaborative Virtual Testing (CVT), i.e. a central web server or data hub, which acts as a repository of archived simulation and conduit for live strain analysis. Each item will be described in the following paragraphs.

Virtual Testing

Virtual testing and GENOA lie at the heart of DPS. Together, they provide an ability to evaluate component behavior, identify maximum strain thresholds and predict failure. GENOA integrates nonlinear finite element structural analysis; composite micro-mechanics; and fracture mechanics to scale up the effects of local damage mechanisms to the structure level and evaluate overall performance and integrity. Virtual testing with GENOA uses material test data, and uncertainty at the micro level, to simulate structural level damage initiation, damage growth, and damage propagation processes. In this manner, changes in structural load paths with damage progression are accurately identified based on physics and material properties. With GENOA, DPS may confidently compare live data from a composite bridge to simulated data generated by an accurate finite element model that replicates the composite bridge and all applicable loads.

Embedded Sensors and Optical Fiber Interrogation

The Fiber Bragg Grating (FBG) sensor has become the most commonly adopted form of fiber optic sensing for structural applications due to its small size. When coupled with a standard interrogation unit, up to one hundred Fiber Bragg sensors may be employed within a single strand, which in turn would be either embedded within the bridge during fabrication or mounted on the surface. If the fiber sensor is strained or pulled from each end of the FBG, planes within the sensor will shift apart and the wavelength that gets reflected will increase. By knowing the unstrained FBG wavelength, one can directly calculate the strain on the fiber at the point where the FBG resides from the wavelength shift of the reflected light. The strain at many points within a fiber can be obtained by monitoring the wavelength of multiple sensing elements dispersed along the fiber.

The DPS Fiber Sensor Interrogator (FSI) system is used for reading real-time strain and temperature data from an array of multiple FBG sensors along a single channel. When ready to extract data, the FSI transmits a broad band light pulse into the fiber in order to illuminate the FBG sensor array. Next, it provides amplification and time-based gating of the reflected sensor signals and examines each sensor's peak reflected wavelength to measure strain. Finally, each sensor peak wavelength is ported to a secondary communication device for delivery to the outside world.

Data Transmission

Reliable data communication is essential for the success of the DPS. For that reason, redundancy and robustness are key criteria for the final system. Currently, DPS utilizes a cellular communications network with a web server to route data from the FSI through an Internet Service Provider (ISP) and on to CVT. Additional protocols are in place and under development. These include an existing communications system that utilizes traditional cellular telephone pc-card technology to allow modem-to-modem communication over a standard cellular telephone network and a proposed commercial satellite communication system that will utilize off-the-shelf hardware to communicate directly with the CVT while employing sophisticated data compression and encryption routines coupled with scheduled or event-driven data deliveries to reduce the shear volume of data and lower the overall cost of transmission.

Collaborative Virtual Testing, central data hub

Collaborative Virtual Testing (CVT) software was developed to facilitate cooperation among geographically dispersed team members. As such, CVT capabilities include conducting secure net meetings; uploading test data; storing presentations, reports, and publications; generating simulation input; running advanced engineering simulations; viewing simulation results; and sorting and searching historical simulation within the archive. More to the point, CVT was designed to allow widely distributed users to run GENOA models on the Internet and share access to results. Access to CVT is controlled by private user accounts with tight security features. Administrator defined user privileges dictate the extent to which a given user may have access to archived simulations. When combined with DPS, CVT becomes a central data hub, accessible to anyone with appropriate credentials, where live data from the field is compared in real time to simulated strain values associated with archived modules. More importantly, CVT provides DPS with a suite of intelligent tools and custom interactive software to compare data, recognize damage, identify the mechanisms that precipitated damage, determine post-damage residual stiffness and residual strength, recognize material sensitivities and propose logical repair solutions.

Proposed Areas of Growth

DPS has been designed to exploit the best features of the core technologies and deliver an interactive tool that can be used on-site or in the laboratory. Yet, new capabilities and modifications are being examined all the time. In the future, data delivery from the remote location may include displacement, rotation, environmental conditions, type of damage, location of damage, degree of damage, and intelligent vehicle identification that occurs either before or during a bridge crossing. Finally, in its current configuration, data is pushed from the remote structure to the CVT evaluation center. Because of the inherent restrictions of satellite technology, engineers at the CVT will be given the ability to pull data from the interrogation unit on demand or identify a schedule for data delivery where load/strain events are captured, encrypted, compressed and stored locally before being delivered on a hourly, daily, weekly or monthly basis. As such, with regard to power consumption, the interrogation box may automatically move to sleep mode until awakened at an appropriate time for a load event.

3. Results and discussions

3.1 *DPS: Case Study*

In a series of tests conducted at the University of California at Irvine (UCI), DPS was presented with a real world application involving the four-point bending of a simply supported composite bridge section. As indicated in Figure 2, the actual specimen was fabricated at Gulfport, Mississippi by Seemann Composites, Inc. To capture the strain data, optical fiber sensors were embedded in the beam during actual fabrication. The beam was 53 inches in length and consisted of a tension rail, four foam bulkheads and a balsa wood core that were all wrapped in a carbon fiber. After the individual components were bonded together, the entire assembly was wrapped in carbon fiber sidewalls. The unit was then shipped to UCI for testing.

Figure 3 shows the conceived test configuration and Figure 4 shows the actual test setup. The delivered specimen included fourteen optical fiber sensors. Eleven were embedded in the specimen and three were mounted on the surface. The sensors were divided between two optical fiber strands, or cables, that extended about three feet from the body of the specimen. After carefully placing the specimen in the test frame with the appropriate fixturing, the two optical fiber lines were connected to the FSI box for interrogation and data broadcast. The FSI box was in turn connected to a desktop computer by way of an Ethernet connection. Prior to testing and broadcasting, the test operator configured the FSI box to identify the location of the sensors and establish the proper connection protocol with the cellular network and ISP. Figure 5 provides a close up image of the FSI box with channels one and two occupied by the optical fiber lines from the specimen.

Load was applied to the specimen through a 55 kips servo-hydraulic actuator manufactured by MTS Systems Corporation. Although a full suite of automated software supported the actuator, the test program was conducted in manual control with the test operator utilizing both force and displacement control modes to position the actuator head and apply load to the beam. Simultaneous to the preparations in the laboratory, a CVT operator, in another location, loaded a model of the bridge onto the system, specified the sensors to be read, and activated a tool within CVT, which readied the system for the retrieval of live data. Figure 6 highlights this process.

Once the actuator head was in position and the CVT was initialized to accept data, the test operator moved to the desktop and commanded the FSI to begin capturing, recording and broadcasting data from the optical fiber sensors. With all data related devices activated, the next task of the test operator was to apply live load to the specimen as shown in Figure 7.

Load was applied in one thousand pound increments from zero to ten thousand pounds. Immediately and in response to this activity, the CVT launched a window that depicted live strain values for each sensor in the form of a dark green curve placed in a chart that plotted strain versus time. The process is shown in Figure 8. A light green curve and a bright red line augmented each chart. The light green curve corresponded to simulated strain for the given location in the bridge and the red curve represented maximum threshold strain generated by simulation for the same physical location. Here, all simulated values were extracted from the GENOA analyses of the FEM model.

Under initial loading, the DPS showed a slight discrepancy between live test data and simulated values. However, once a significant load was applied to the system, i.e. in excess of 3000 pounds, less noise was in the system and the live data and the simulated data showed excellent correlation for all sensors. In this region, the discrepancy between live data and simulated for all three sensors was within ten percent. Figure 9 provides a close up value of one of the charts during testing.

In general, simulated data was in good agreement with live data. Since the test did not exceed ten thousand pounds, which is well within the working range of the actuator and the beam, it was assumed that damage did not occur anywhere in the specimen. However, to highlight the warning system associated with DPS, the test operator utilized an interactive feature within the tool that allows a user to adjust the value and location of the red line in terms of percentage of maximum threshold strain. In this way, an operator would be able specify that a warning light should be triggered if a specimen experiences strain that is, for example, sixty percent of the maximum threshold value. Figure 10 shows this feature.

3.2 *Structural Evaluation of the Temporary Field Repair System*

In order to evaluate the effectiveness of a general repair system, three tests were performed on three specimens that were cut from the modules of a prototype composite bridge. The dimensions of each specimen were 8" (0.2 m) by 48" (*1.22 m*). The "undamaged" specimen was used as a "control" specimen and was tested to failure in order to determine the ultimate failure load and failure strain, as well as, identify the mode or modes that triggered failure. The second test was performed on the damaged specimen, whose area of adulteration corresponded to severe damage to the top carbon/epoxy face and severe damage to the balsa core. Figure 11 shows the size, geometry and location of the damaged area. The objective of the second test was to determine the residual stiffness and strength of the partially damaged specimen as compared to both the undamaged and the repaired specimens. The third test was performed on a repaired specimen, see Figure 12, that was identically damaged as specimen two but was later repaired using temporary field repair procedures. The repair process consisted of filling the engineered void, i.e. damage, with a two to one mixture of find sand and then bonding a single layer of thin cross-ply cloth over the surface of the specimen, so that the wound is completely covered.

All specimens were tested in a 4-point flexural loading configuration. Two line loads were applied at a distance of 6" (152.4 mm) from the center of each specimen. The loads were applied in the form of a ramp with a loading rate of 2 kips/min (8.9 kN/min) and were performed up to failure as shown in Figure 13. All specimens were instrumented by both electrical strain and deflection gages. Elastomeric pads were placed at the supports and the line load applications, in order to avoid premature failure due to the expected high stress concentration at theses locations. Figure 14 shows the typical setup for all specimens.

The behavior of the undamaged specimen was linear up to a load level of 13 kips, after which, slight gradual stiffness degradation was observed as shown in Figure 15. The ultimate failure load was 24.13 kips (107.33 kN) with a maximum deflection at the mid-span of 0.57" (14.48 mm) with an initial stiffness of 38 kip/in. The mode of failure was brittle in the form of local debonding, in the *unsupported* right portion of the specimen between the right support and the line load, followed by a local buckling as shown in Figure 16. Simultaneously, the balsa wood core failed suddenly including the splitter, or intermediate laminate. No failure was observed in either the top or bottom composite face sheet.

The damaged specimen was tested using the same setup as the undamaged specimen, which is depicted in Figure 17. From the start, this specimen showed a lower stiffness as compared to the control specimen with an average initial linear stiffness of about 15 kip/inch. The ultimate load of this specimen was 18.24 kips (81.13 kN) which was about 75% of the ultimate capacity of the undamaged specimen. The corresponding mid-span deflection at the ultimate load was slightly larger than the corresponding deflection of the undamaged specimen *(0.61" (15.5 mm) vs. 0.57" (14.48 mm))*. Unlike the undamaged specimen, the failure was initiated at the pre-damaged area located between the two line loads. This can be attributed to the major reduction of the area and stiffness of the compressed face sheets at the damaged area.

The first mode of failure was a compression failure of one of the two 2" X 8" *(51 mm X 203 mm)* top face sheets at the neighborhood of the right line load as shown in Figure 18. As a result, debonding of the face sheet at the damaged region occurred followed by delamination of this portion of the face sheets, which extended 3" (76 mm) from the line load. At the same time, local damage to the balsa core was observed. Load versus mid-span deflection for the damaged specimen is shown in Figure 19.

For the repaired specimen, the test setup was, once again, identical to the setup used for both the undamaged (*control*) and the damaged specimen. This setup is shown in Figure 20. As compared to the other two specimens, both the initial and the average flexural stiffnesses of the repaired specimen were relatively higher. In general, the behavior was linear up to the failure load that was reached at 27.94 kips (*124.3 kN*) as shown in Figure 21. Thus, the strength of the repaired specimen was 16%, and 53.2% higher than the flexural strength of the undamaged and damaged specimens, respectively. The maximum mid-span deflection at the ultimate load was 0.55" (*13.9 mm*) which is slightly smaller that the corresponding deflection of both the undamaged and damaged specimens. The average stiffness of this specimen was 50.8 kip-in, which is 338% of the average stiffness of the damaged specimen and 133% of the original undamaged design as indicated in Figure 22. In conclusion and based on the experimental

results, the repair procedures was very effective in not only restoring the original capacity, but also resulted in a 16% increase in the strength of the original design. In addition, the repair procedure upgraded the flexural stiffness more than 3.4 fold as compared to the stiffness of the damaged stiffness shown in Figure 23. The ultimate failure of this specimen was initiated by debonding of the top balsa core from the intermediated separation laminate. This was followed by localized core failure at different locations as shown in Figure 24.

4. Conclusions

This paper presented the results of an on-going program that is developing novel techniques to monitor and repair composite bridges. Following the introduction, Section 2 provided background information on progressive failure, GENOA, and diagnostic monitoring of remote structures, which explained how the individual components provided a foundation for DPS. Section 3.1 exposed the DPS to a real world application. In general DPS functioned effectively. Data from the test article was delivered to the CVT and compared to simulation data from a corresponding GENOA model. The two sets of data exhibited good correlation and were not encumbered by delays or other technical challenges. Once system noise was reduced, the average error between the live data set and the simulated data set did not exceed ten percent. Results suggest a full suite of verification examples would be useful when describing and defending the efficacy of the DPS. Further evolution of the tool in terms of redundant data transmission and expanded interactive software is warranted.

Section 3.2 focused on the evaluation of temporary repair techniques. Here, experimental results showed the repaired specimen performed significantly better than the undamaged and damaged specimen in all observed categories. This result called into question the fundamental quality and merits of the original design of the composite chord and by default the composite deck, which, in turn, is a major component of the composite bridge. The findings indicates that the original design of the composite bridge can be further optimized, since the limit-state is *debonding and core strength* rather than the *strength of the composite top face sheet.* It should be noted that the thickness of the repair laminate was more than 10 times less than the thickness of the original face sheets. Despite this reduction the strength and stiffness of the repaired specimen were higher than those of the original approach. Beyond design, it is recommended that further testing with alternative repair procedures should be undertaken. A qualitative assessment of competing rehabilitation methodologies would be a valuable contribution to the repair knowledge base. In addition, the next generation of repairs should utilize DPS by employing intelligent fiber optic patches or traditional embedded fiber optic sensors wherever possible.

5. Acknowledgements

This work is a part of a multi-phase SBIR research project funded by the U.S. Army Tank Automotive Research, Development and Engineering Center (TARDEC) to develop methodologies for the repair and health monitoring of composite bridges. This effort has utilized the expertise of the University of California at Irvine, Seemans Composites and Insensys Corporation to develop advanced tools and technologies to support that endeavor. The

information reported in this paper reflects the authors' opinions and does not necessary imply endorsement of the sponsoring agency.

References

1. Abdi, F., Surdenas, J., Mosallam, A. and Wang, J.J. *Field Repair Technology For Composite Bridges, Phase I Final Report, Submitted to U.S. Army TACOM*, 2003.
2. *Advanced Composites for Bridge Infrastructure Renewal- Phase II, DARPA Agreement 0030, Volume II-Task No. MDA972-94-3-14*, Submitted to DARPA by Advanced Composites Technology Transfer/Bridge Infrastructure Renewal Consortium, 2000.
3. Chamis, C.C. *Failure Criteria for Filamentary Composites, Composite Materials Testing and Design: ASTM STP 460*, 1969 (American Society for Testing and Materials)
4. Chamis, C.C., and Sinclair, J.H. *Micromechanics of Intraply Hybrid Composites: Elastic and Thermal Properties*, 1979 (NASA TM-79253).
5. Hill, R. *The Mathematical Theory of Plasticity*, 1950 (Oxford University Press, Oxford).
6. Morrow J. *Fatigue Design Hand book*, 1968 (Society of Automotive Engineers, Graham).
7. Mosallam, A. S. and Haroun M.A. Structural Evaluation, Repair and Construction of a Composite Highway Bridge Deck, *2nd International Workshop on Structural Composites for Infrastructure Applications, NSF/HBRC*, Cairo, Egypt, December 17-18, 2003.
8. Mosallam, A., Ramki Iyer, and Abdi, F., *Progressive failure analysis of composite army bridge*, 2005 (CICE Publications Australia).
9. Murthy, P.L.N. and Chamis C.C. *Integrated Composite Analyzer (ICAN): Users and Programmers Manual*, 1986 (NASA Technical Paper 2515).
10. Nakazawa, S., Dias J.B., and Spiegel M.S. *MHOST Users' Manual, Prepared for NASA Lewis Research Center by MARC Analysis Research Corp*, 1987
11. Ramki Iyer, Mosallam, A., and Abdi, F. Progressive failure analysis of Composite Army Bridge, *The Second International Conference on FRP Composites in Civil Engineering* 8-10 December, Adelaide, Australia, 2004
12. Tsai, S. W. (1968). Strength Theories of Filamentary Structures, in *Fundamental Aspects of Fiber Reinforced Plastic Composites*, edited by R.T. Schwartz and H.S. Schwartz, Eds., Interscience, New York.

Diagnostic Component

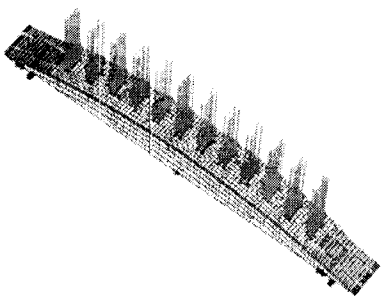

Step 1

Run Model with GENOA

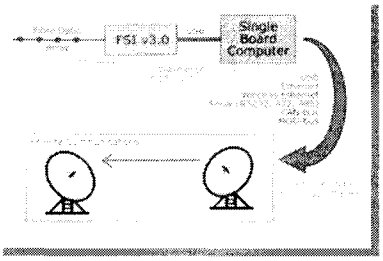

Step 2

Send Live Data from Bridge

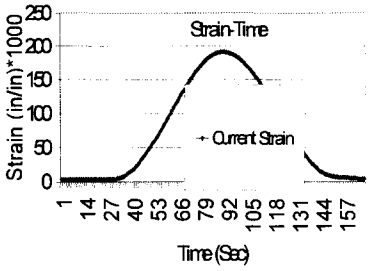

Step 3

Receive Live Data from Bridge

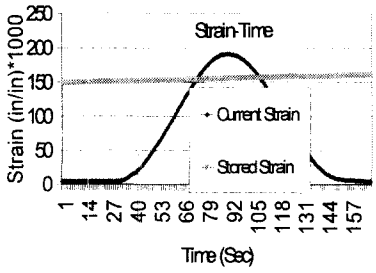

Step 4

Compare Live Data to Stored Data

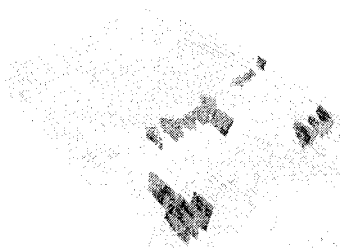

Step 5

Multi-site Damage Assessment

Identify Location of Damage and Corresponding Load or Cycle Number

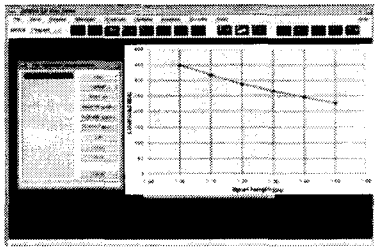

Step 6

Evaluate Residual Stiffness & Strength

Run Material Characterization Analysis (MCA) with Residual Damage to plot/find Residuals

Prognostic Component

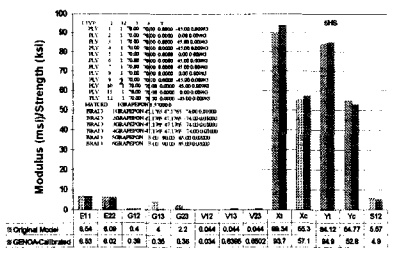

Step 7

Assess Available Materials for Repair

List Available Repair Material in Databank
Plot Corresponding Strength and Stiffness

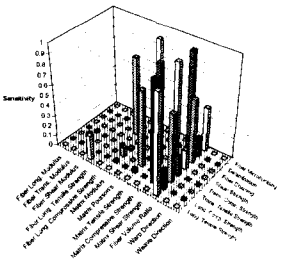

Step 8

Suggest Materials for Repair

Run Material Uncertainty Analysis (MUA) to Find Material Failure Sensitivity and Suggest Percentage Mix of Constituents

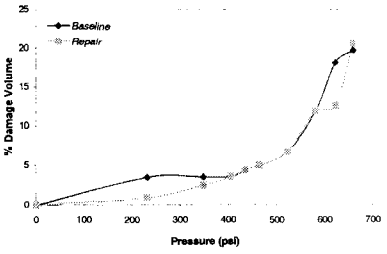

Step 9

Evaluate/Compare Performance of Baseline versus Repaired Specimen

Figure 1 - DPS System Step by Step

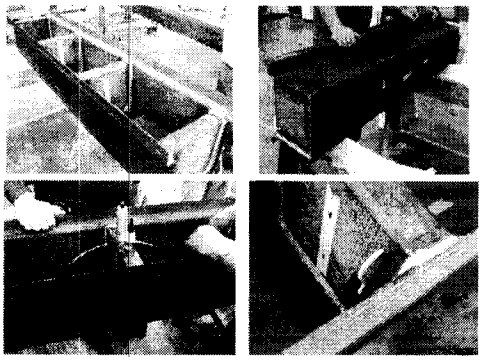

Figure 2 Optical Fiber Installation

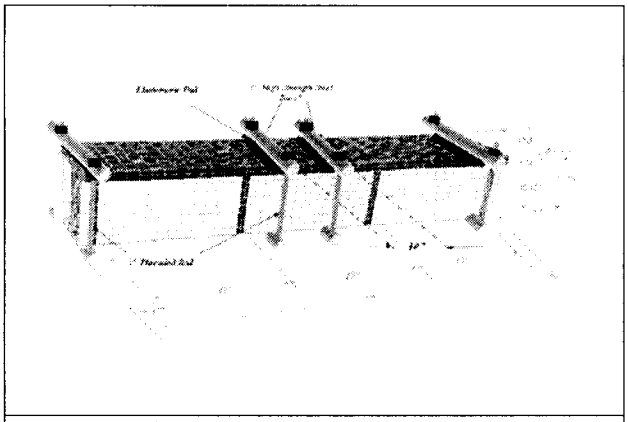

Figure 3 Test Configuration

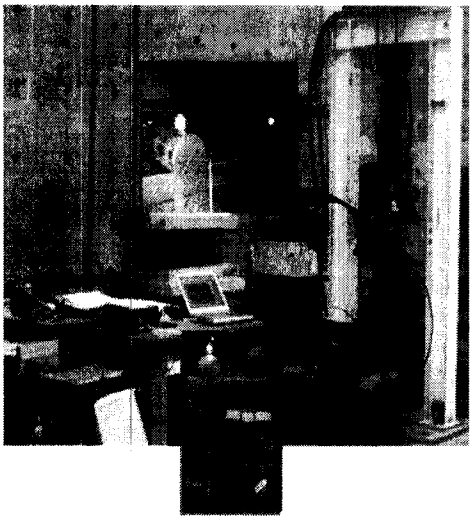

Figure 4 Actual Test Setup

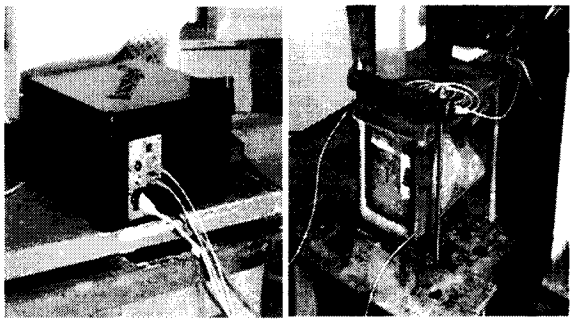

Figure 5 FSI and optical fiber sensors

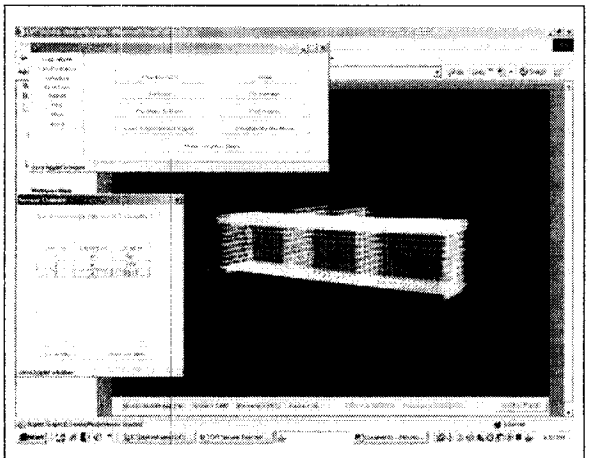

Figure 6 Model loaded for data delivery

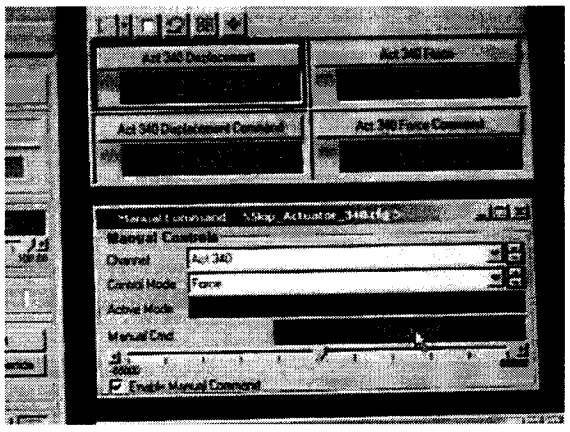

Figure 7 Command given to actuator

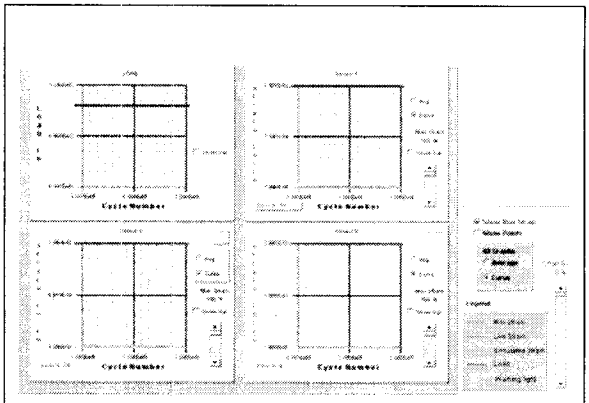

Figure 8 Strain values from load

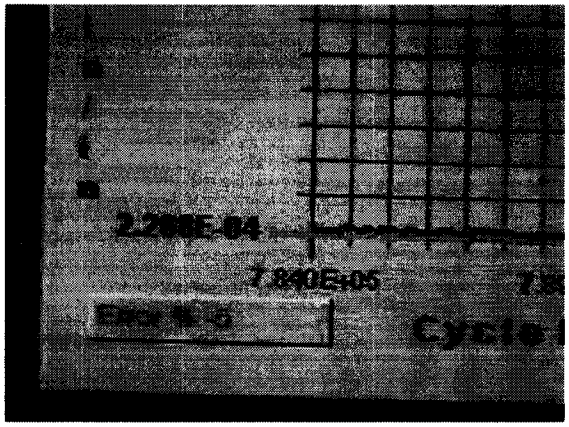

Figure 9 Error output by DPS

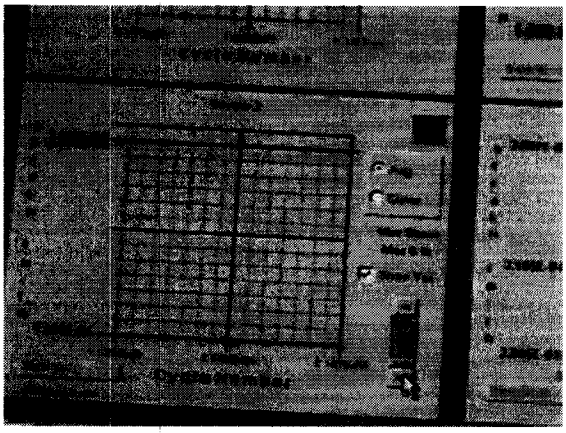

Figure 10 Strain triggering red

Figure 11 Damaged Top Chord Geometry

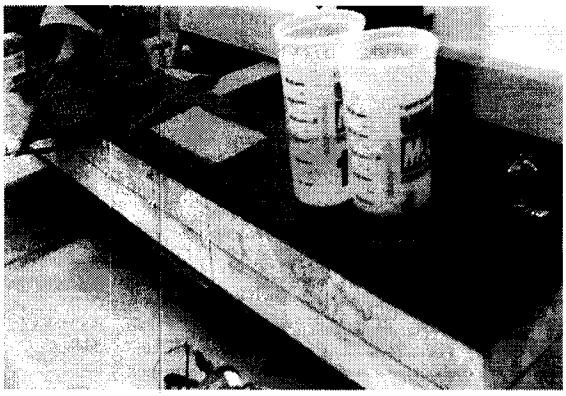

Figure 12 Repair of Damage

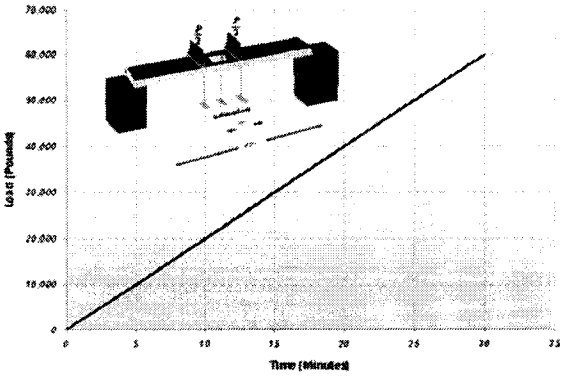

Figure 13 Rate of Load Application

Figure 14 Test Setup for Chords

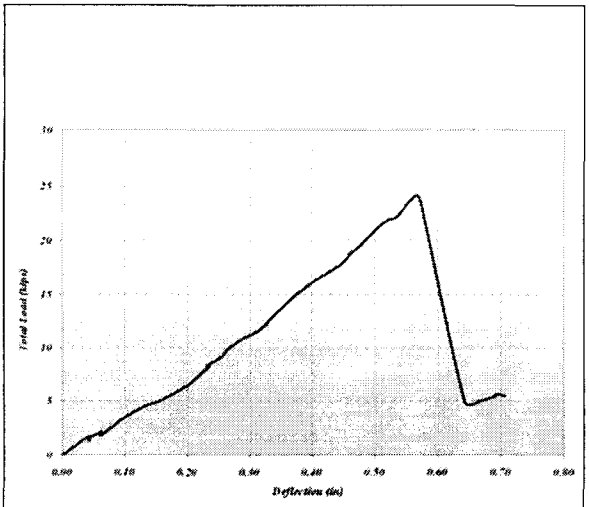

Figure 15 Load vs. Deflection Undamaged

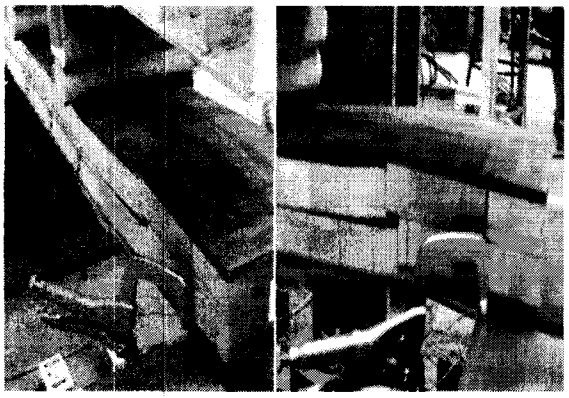

Figure 16 Failure Mode Undamaged

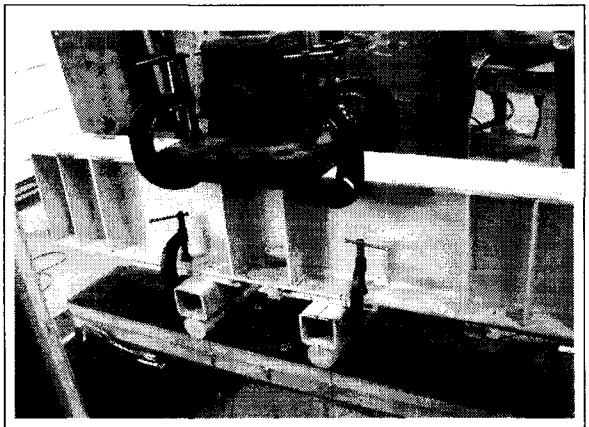

Figure 17 Test Setup for Damaged

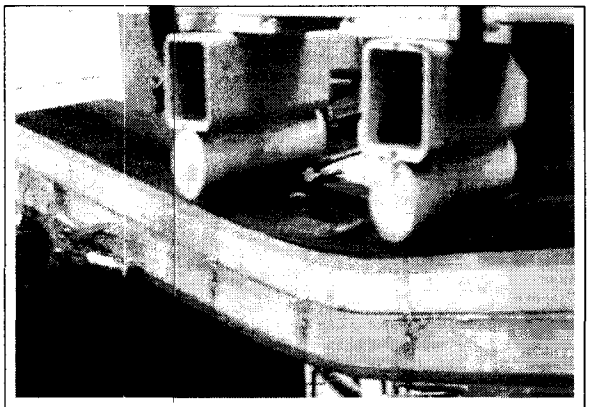

Figure 18 Failure Mode Damaged

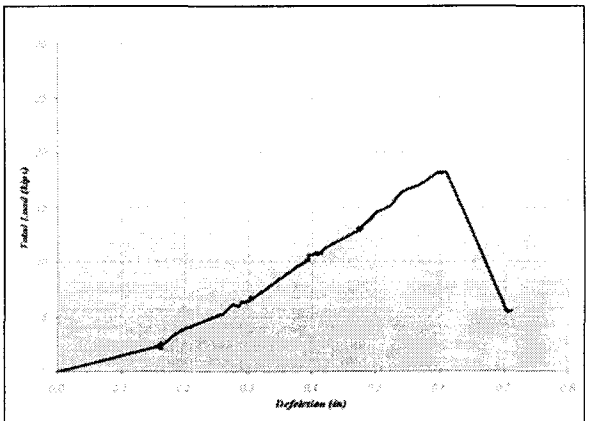

Figure 19 Load vs. Deflection Damaged

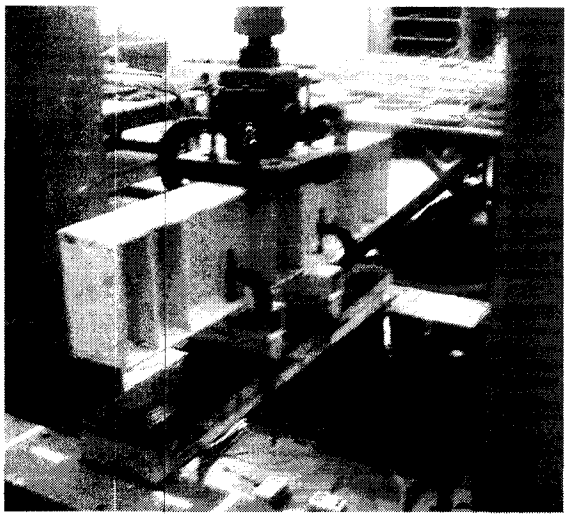

Figure 20 Test Setup for Repaired

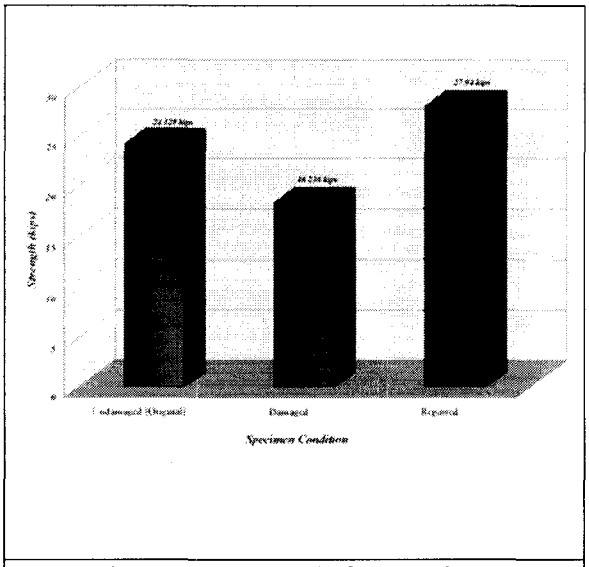

Figure 21 Strength Comparison

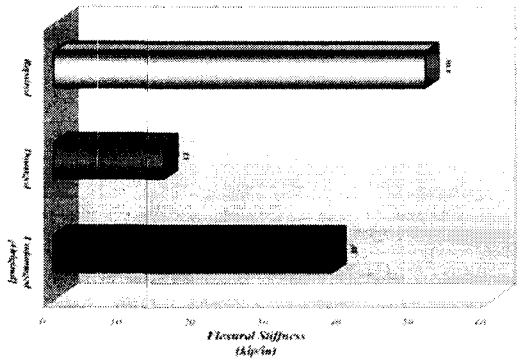

Figure 22 Stiffness Comparison

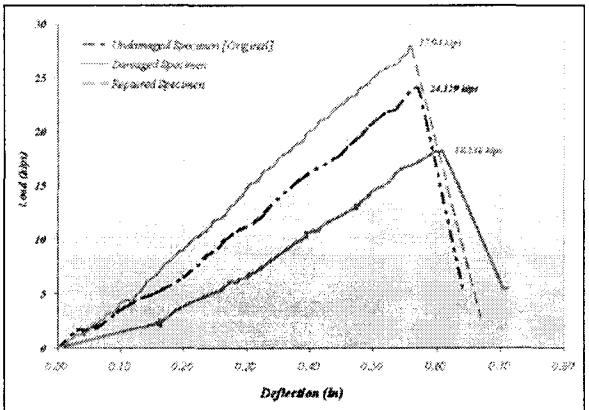

Figure 23 Load vs. Deflection: All

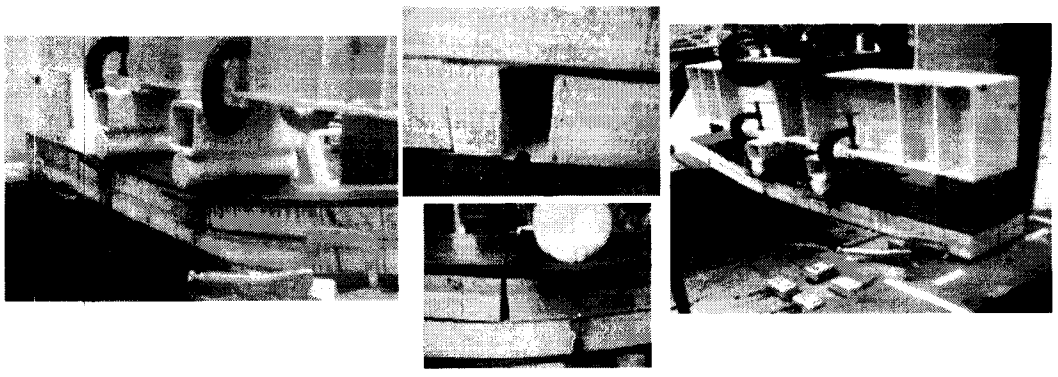

Figure 24 Progression of Failure in the Repaired Specimen